Supplementary Materials for "Small Nuclear Quantum Effects in Scattering of H and D from Graphene"

Hongyan Jiang*,[1] Xuecheng Tao*,[2] Marvin Kammler,[1] Feizhi Ding,[2] Alec M. Wodtke,[1,3,4] Alexander Kandratsenka,[1] Thomas F. Miller III,[2] and Oliver Bünermann[1,5,4]

[1] *Department of Dynamics at Surfaces, Max-Planck-Institute for Biophysical Chemistry, Am Faßberg 11, 37077 Göttingen, Germany*

[2] *Division of Chemistry and Chemical Engineering, California Institute of Technology, Pasadena, California 91125, USA*

[3] *Institute for Physical Chemistry, Georg-August University of Göttingen, Tammanstraße 6, 37077 Göttingen, Germany*

[4] *International Center for Advanced Studies of Energy Conversion, Georg-August University of Göttingen, Tammanstraße 6, 37077 Göttingen, Germany*

[5] *Institute for Physical Chemistry, Georg-August University of Göttingen, 37077 Göttingen,, Tammanstraße 6, 37077 Göttingen, Germany*

A. MODIFIED GFN-xTB HAMILTONIAN

For the purpose of studying the scattering dynamics of H and D from graphene, it was necessary to modify the GFN-xTB Hamiltonian [1], originally developed for near-equilibrium geometries. Following Eq. 16 in Ref. 1, the potential energy of the system is

$$E_{\mathrm{GFN-xTB-mod}} = E_{\mathrm{GFN-xTB}} + E_{\mathrm{RE}} \tag{S1}$$

with

$$E_{\mathrm{RE}} = \sum_{\mathrm{A}}^{\mathrm{atoms}} \mathrm{CN_A}\, f_{\mathrm{A}}. \tag{S2}$$

f_{A} is the element-specific atomization correction energy, and $\mathrm{CN_A}$ represents the coordination number for atom A [2], defined as follows.

$$\mathrm{CN_A} = \sum_{\mathrm{B}\neq\mathrm{A}}^{\mathrm{atoms}} \left(1 + e^{-\lambda[\mu(R_{\mathrm{A}}+R_{\mathrm{B}})/r_{\mathrm{AB}}-1]}\right)^{-1} \tag{S3}$$

$R_{\mathrm{A/B}}$ and r_{AB} are the covalent radius of atoms A/B and the distance between atoms A and B, respectively. We fit f, λ and μ to benchmark density functional theory (DFT) calculations at the B3LYP/cc-pVDZ/JKFIT [3–6] level, with reference configurations consisting of an H atom interacting with a $C_{42}H_{16}$ graphene cluster. Values for the optimized parameters are reported in Table I.

Fig. S1(a) shows the minimum energy path (MEP) for an H atom's perpendicular approach to a carbon atom on the graphene flake, comparing the B3LYP and optimized GFN-xTB-mod energies. Fig. S1(b) shows the two-dimensional cut through the high dimensional potential energy landscape, with all other degrees of freedom are allowed to relax at each C-H distance. The ability of GFN-xTB-mod to reproduce the B3LYP barrier and well-depth is remarkably good. Furthermore, its use accelerates the dynamics calculations of this work by one-thousand fold, compared to calculations with a hybrid functional. This allows the GFN-xTB-mod approach to be further tested by simulations of experimental scattering distributions, where good agreement is also seen. See the main text.

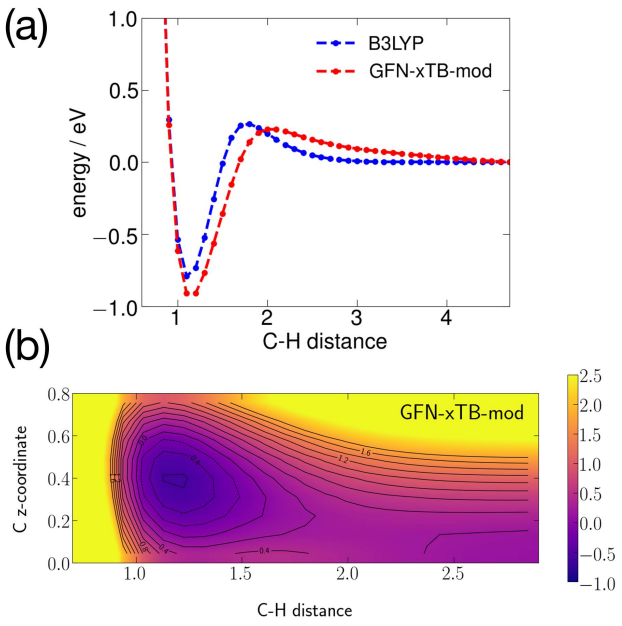

FIG. S1. **The minimum energy pathway (MEP) for the perpedicular approach of an H atom on top of a carbon atom on the graphene flake.** (a) Comparing the one-dimensional surface at the GFN-xTB-mod and B3LYP/cc-pVDZ levels of theory as a function of the C-H distance, with all other degrees of freedom optimized at each C-H distance. (b) Using GFN-xTB-mod, the two-dimensional surface as a function of the C-H distance and the displacement of the interacting C atom from the plane of the graphene flake, again with all other degrees of freedom optimized. All energies are in eV.

TABLE I. Results for the reactive energy term that describes C-H interaction, as defined in Eqs. S2 and S3.

Parameters	Value	Parameters	Value
f_{H}	0.6448 eV	λ	7.141
f_{C}	0.0261 eV	μ	1.144

B. TRANSITION STATE THEORY ESTIMATION OF THE ISOTOPE EFFECT

To investigate the isotope effect in the H/D-on-graphene reactive system, we first employ the Rice–Rampsberger–Kassel–Marcus (RRKM) rate theory [7] — a standard microcanonical transition state theory (mTST) — to compare the difference between the chemisorption rates of H and D atom onto the surface, respectively. The RRKM is applied in a microcanonical manner consistent with that laid out in Ref. 8 for surface collisions. We assume that the rate-determining step in the chemisorption is a unimolecular process where the reactant is an activated pre-cursor complex (PC) [9] that corresponds to the H/D atom in a physisorbed complex with the surface at a distance 4Å [10]. Activated PC is also assumed to have sufficiently rapid intramolecular energy distribution such that the statistical mechanical treatment in mTST is applicable.

The RRKM microcanonical rate is

$$k(E) = \frac{N^{\ddagger}(E - E^{\ddagger})}{h\,\rho_{\mathrm{PC}}(E)}. \tag{S4}$$

Here $N^{\ddagger}$ is the transition state sum of states, $E^{\ddagger}$ is the energy difference between the PC and the transition state geometry (including zero-point energy contributions), and ρ is the PC density of states. Note that the PC consists of a structureless H/D atom and the C atoms that vibrate at the graphene phonon frequencies with no chemical interactions to the H/D atom. As a result, the denominator in the Eq. S4 is solely determined by the graphene phonon frequencies and the isotopic difference of the microcanonical rate then becomes

$$\frac{k_{\mathrm{D}}(E)}{k_{\mathrm{H}}(E)} = \frac{N^{\dagger}_{\mathrm{D}}(E - E^{\dagger}_{\mathrm{D}})}{N^{\dagger}_{\mathrm{H}}(E - E^{\dagger}_{\mathrm{H}})}. \tag{S5}$$

Fig. S2 presents the microcanonical rate ratio of the H/D chemisorption, obtained by calculations with Eq. S5 on the GFN-xTB potential energy surface. The sum of the states in Eq. S5 is calculated with the Beyer-Swinehart algorithm [11] at the level of separable harmonic vibrations. It is predicted that a large isotope effect more than 250% favors D sticking is observed, in contrary to the experimental observation of almost no isotope effect. The inconsistency

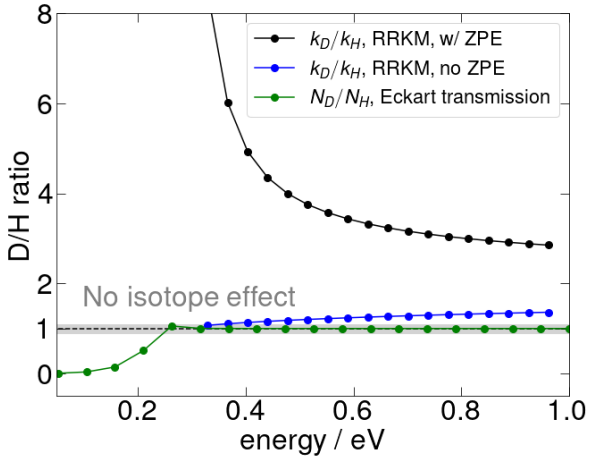

FIG. S2. **Isotope differences in the H/D-on-graphene scattering events predicted with theories at different levels. The ratio of microcanonical transition state theory rates (mTST, Eq. S5, with and without the inclusion of the zero-point energy (ZPE) in the transition state complex) and Eckart barrier transmission probabilities are presented to examine the isotope effect. The filled grey area indicates no isotope effect.**

between the mTST result and the experiment measurement emphasizes the highly non-equilibrium nature of the chemisorption process in the scattering experiment and the ultrafast reaction timescale that prohibits a sufficient energy redistribution of the reactive system, which leads to this particular breakdown of the statistical rate theory. Furthermore, the approximation of those non-phonon active modes as harmonic vibrations might also degrade the accuracy of mTST result. To this end, those inadequacies in the mTST modelling urges the need for an appropriate inclusion of the dynamical effects and vibrational anharmonicity in the simulation of H/D-on-graphene scatterings.

As a simplified alternative, we also estimate the isotopic difference between H and D atom transmission through the adsorption barrier with the one-dimensional Eckart barrier model. [12, 13] The result is also presented in Fig. S2. Significant difference is shown at lower incidence energies between the transmission probabilities that the scattering system tunnels through the adsorption barrier; while at the energies that higher than the barrier, Eckart barrier model predicts exactly the same classical transmission for H/D atoms and no isotope difference is seen. This reduced-dimensional transmission model is extremely intuitive to describe the scattering process, however is also a grossly oversimplified one that lacks the capability to describe the collective graphene motions which are orthogonal to the reaction coordinate. The latter has proven to be essential for quantitatively understanding the reactivity in the H/D scattering on the graphene surface. [14]

C. TRAJECTORIES AND COMPARISON TO EXPERIMENT

Trajectory calculations (cMD or RPMD) were initialized following the procedure in Ref. 14 For a given incidence energy E_i and angle ϑ_i at which comparison with experiment is to be made, the following steps are performed.

(1) The initial configurations of the graphene flake are sampled from a trajectory propagated using either with cMD or RPMD and thermalized at the experiment's temperature of 300 K. More specifically, the trajectory is pre-equilibrated for 40 ps and then propagated for another 30 ps, during which initialization geometries are sampled.

(2) The collision point of H/D atom on the surface ($x_o, y_o, z_o = 0$ Å) is randomly selected from within the center unit cell of the graphene flake.

(3) The azimuthal scattering angle φ_i is drawn from a uniform distribution between $[0, 2\pi)$.

(4) The initial height of the projectile atom is set at 4 Å from the surface. The (centroid) position to initialize the projectile atom (x_i, y_i, z_i) is then calculated using (x_o, y_o, z_o), ϑ_i and φ_i, i.e.

$$\begin{aligned} x_i &= x_o + (z_i - z_o)\tan\vartheta_i \cos\varphi_i, \\ y_i &= y_o + (z_i - z_o)\tan\vartheta_i \sin\varphi_i, \\ z_i &= 4\,\text{Å}. \end{aligned} \tag{S6}$$

(5) The magnitude of the H/D atom's velocity vector is calculated from E_i, and its direction is found geometrically by connecting a line between the initial position of the H atom and the collision point.

(6) The relative positions and momenta of the internal ring-polymer beads with respect to those of the centroid are thermally sampled at 300 K.

Fig. S3 presents the scattering distribution at ϑ_i between 60° and 30° from experimental measurement and RPMD simulations. They quantitatively agree with each other.

D. EXPERIMENTALLY DERIVED SURVIVAL AND STICKING PROBABILITIES

Experimental data like that of Fig. 2 and Fig. S3 were used to derive the H and D survival probabilities as function of normal incidence translational energy. The experiments are only sensitive to scattered atoms within 2.8° of the plane defined by the incidence atom beam and the surface normal. We integrate over the out of plane scattered flux assuming cylindrical symmetry of the angular distribution with respect to a line coincident with the maximum scattered intensity. This assumption was validated in Ref [15]. Fig. S4 shows the Survival fluxes at incidence angles from 60° to 30° – it increases with ϑ_i, reaching a plateau below $E_n = 0.35$ eV, with $E_n = E_i \cos^2\vartheta_i$ the normal incidence energy. We set the absolute scale of the survival probability to 1 at this plateau. From this, we easily obtain the sticking probabilities shown in Fig. 2.

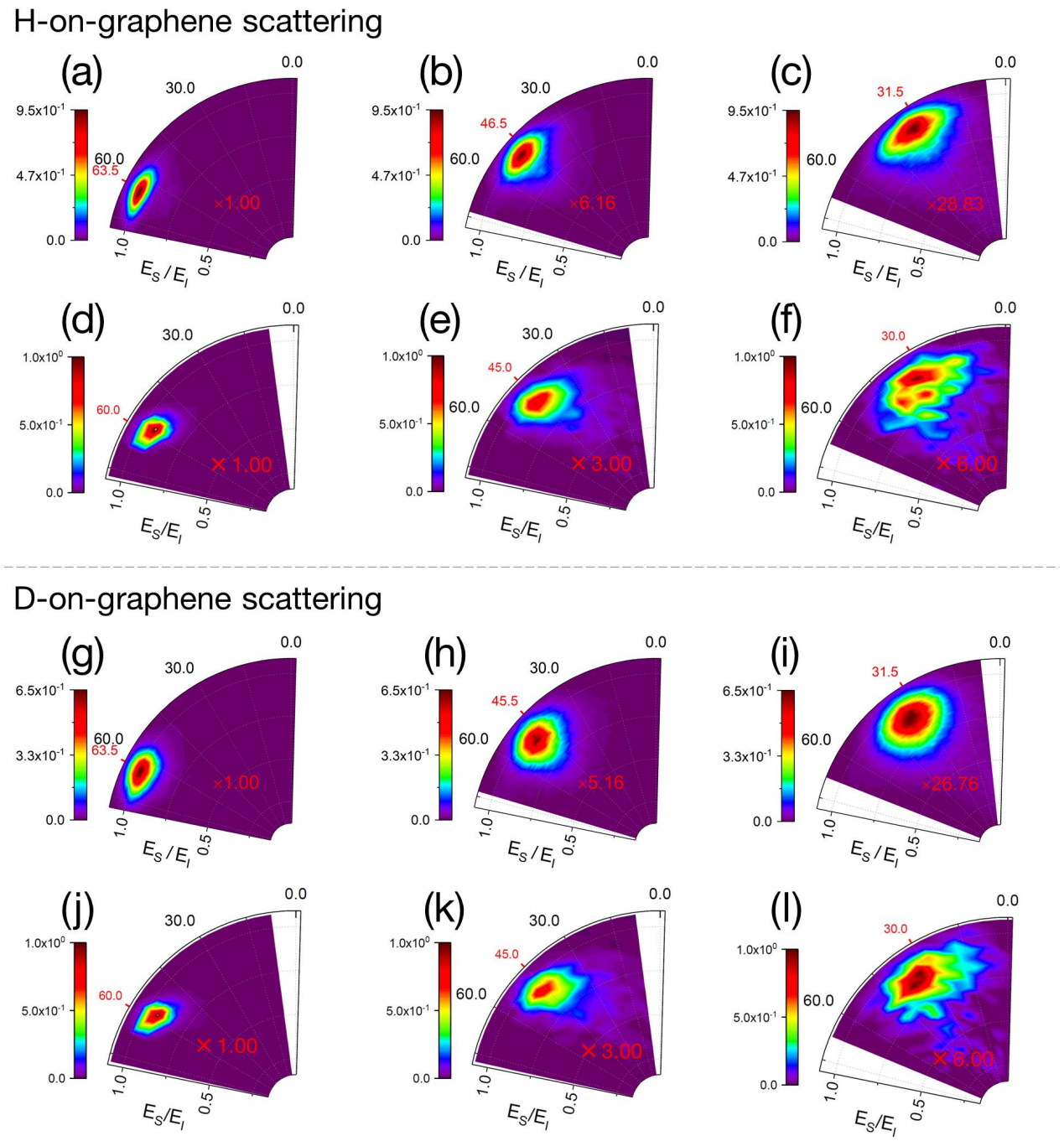

FIG. S3. **Comparing theory with experiment: Scattering distribution of H/D collision with graphene.** (a)-(c) H scattering experiment; (d)-(f) H scattering theory; (g)-(i) D scattering experiment; (j)-(l) D scattering theory. In all figures, the scattering energy, E_s, is shown along the radial coordinate as a fraction of E_i and the scattering angle, ϑ_s, is shown on the polar coordinate. All theoretical scattering distributions were obtained with RPMD trajectories under the influence of GFN-xTB potential energies. Each heat map is multiplied by the indicated number shown in red. We encourage the reader to compare this figure to Fig. S10 of [14]. Such a comparison shows that the new GFN-xTB PES provides an equally accurate representation of the forces during scattering. $E_i = 0.99$ eV for H and $E_i = 0.94$ eV for D scattering experiments.

E. COMPARING GFN-xTB WITH EMFT-REBO POTENTIAL

In this work, we have developed a new PES for the H/graphene system using the GFN-xTB method. Using it, we are able to accurately reproduce experimentally measured H and D atom scattering distributions using cMD and

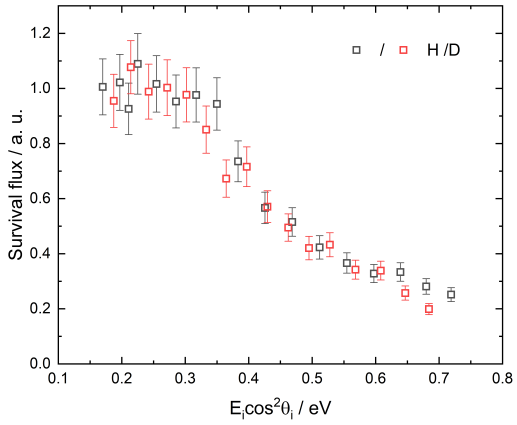

FIG. S4. **Experimentally derived total survival fluxes.**

RPMD. Previously, another PES [14] based on reactive empirical bond order (EMFT-REBO) formalism [17] with training data from quantum embedding calculations [18–20] is also used to describe the graphene electronic structure in the same scattering event. To this end, the current section compares the quality of these two potentials.

Fig. S5 shows the graphene phonon density of states spectra (PDOS) generated from xTB and REBO potential, respectively, compared with the published periodic DFT calculations at the GGA level [16] (black solid line). The phonon power spectrum is calculated as the Fourier transform of the velocity autocorrelation function of the carbon atoms, which is obtained from classical molecular dynamics calculations. The PDOS spectrum obtained from the GFN-xTB PES is shown in red, while that obtained with EMFT-REBO is shown in green. The three theories model a free standing graphene sheet. It is immediately clear that GFN-xTB describes the high frequency phonons of graphene much better than does EMFT-REBO. Furthermore, the phonon band gap between 1000 and 1300 cm^{-1} is not captured by EMFT-REBO. The high frequency phonons so poorly described by EMFT-REBO are attributed to in-plane optical phonons, precisely those so critical to the H sticking process [14].

These deficiencies in the EMFT-REBO PES leads to an absence of significant nuclear quantum effects. Fig. S6 shows EMFT-REBO based sticking probabilities for H and D using both cMD and RPMD trajectories. No difference between classical and quantum dynamics is seen. Contrast this with Fig. 3, which show analogous results using

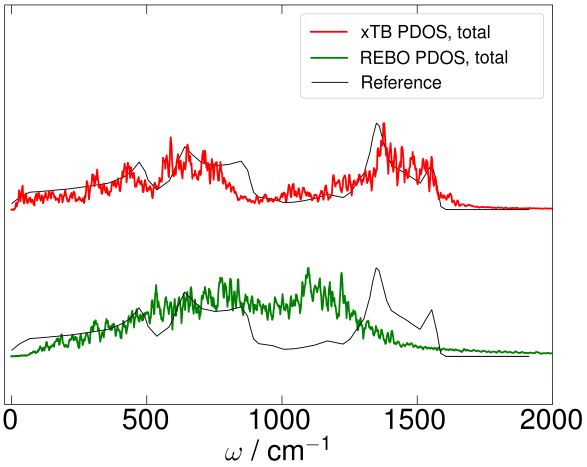

FIG. S5. **Phonon density of states spectrum calculated with GFN-xTB and EMFT-REBO potential at 300 K, respectively.** The phonon power spectrum is calculated as the Fourier transform of the velocity autocorrelation function of the carbon atoms, which is obtained from classical molecular dynamics calculations. Reference spectrum are took from Fig. 5 of Ref. 16.

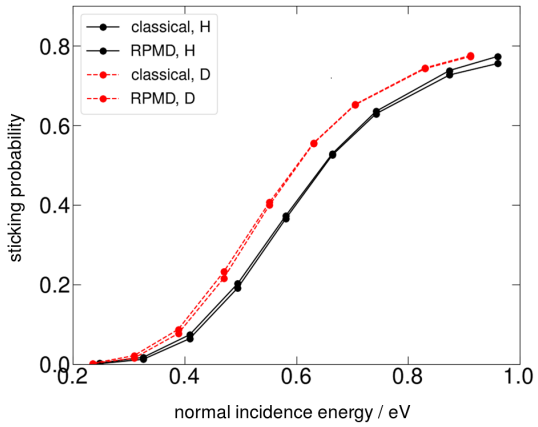

FIG. S6. **Sticking probability of H/D scattering on graphene as a function of normal incidence energy. The calculation is performed using the EMFT-REBO PES reported previously [14].**

GFN-xTB.

F. INTERACTION TIME OF H/D WITH GRAPHENE

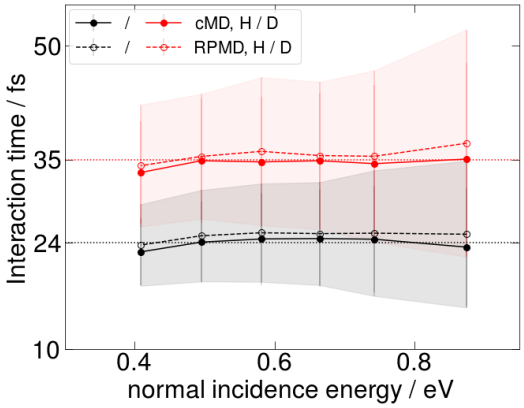

FIG. S7. **Interaction time of the scattered H/D atom with the graphene surface from simulations.** The symbols present the mean value of the interaction time from trajectory statistics and the shadow area in black and red, respectively, present the distribution width. The interacting period is defined that the distance of H/D projectile and the nearest neighbouring C atom is shorter than 2.5 Å.

G. ROBUSTNESS WITH RESPECT TO THE RPMD SIMULATION PROTOCOL

In Fig. S8, classical molecular dynamics (cMD, in black) and RPMD (in red) are reproduced from Fig. 2, with the label $T_{\mathrm{int,H}} = 300$ K indicating the non-equilibrium RPMD method reported in the main text. Also shown are RPMD simulations with the H/D internal ring-polymer temperature is set to $T_{\mathrm{int,H}} = \mathrm{E}_n/k_B = \mathrm{E}_i \cos^2 \vartheta_i / k_B$, following the 'free-particle direct shooting' protocol [21]. All other simulation details in these two sets of RPMD results are kept to be the same. The fact that both RPMD results are in complete agreement indicates that the results reported here are insensitive to the protocol used for initializing the internal temperature of the H/D ring-polymer in the non-equilibrium simulations. This is also consistent with the conclusion from the main text that the NQE associated with the H/D atom is negligible for the sticking dynamics studied here (Fig. 3(a)).

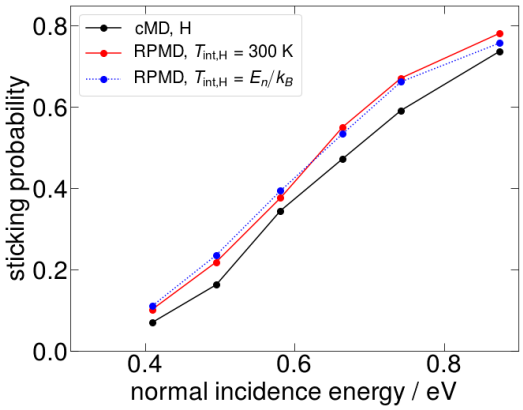

FIG. S8. **H atom sticking probability as a function of normal incidence energy - testing sensitivity with respect to the initialization of the H/D internal ring-polymer temperature.**

[1] S. Grimme, C. Bannwarth, and P. Shushkov, J. Chem. Theory Comput. **13**, 1989 (2017).
[2] S. Grimme, J. Antony, S. Ehrlich, and H. Krieg, J. Chem. Phys. **132**, 154104 (2010).
[3] A. D. Becke, J. Chem. Phys. **104**, 1040 (1996).
[4] C. Lee, W. Yang, and R. G. Parr, Phys. Rev. B **37**, 785 (1988).
[5] A. K. Wilson, D. E. Woon, K. A. Peterson, and T. H. Dunning Jr, J. Chem. Phys. **110**, 7667 (1999).
[6] R. Polly, H.-J. Werner, F. R. Manby, and P. J. Knowles, Mol. Phys. **102**, 2311 (2004).
[7] R. A. Marcus, The Journal of Chemical Physics **20**, 359 (1952).
[8] H. L. Abbott and I. Harrison, The Journal of Physical Chemistry A **111**, 9871 (2007).
[9] M. Bowker, Journal of Physics: Condensed Matter **22**, 263002 (2010).
[10] E. Ghio, L. Mattera, C. Salvo, F. Tommasini, and U. Valbusa, J. Chem. Phys. **73**, 556 (1980).
[11] T. Beyer and D. Swinehart, Communications of the ACM **16**, 379 (1973).
[12] C. Eckart, Phys. Rev. **35**, 1303 (1930).
[13] H. S. Johnston and J. Heicklen, J. Phys. Chem. **66**, 532 (1962).
[14] H. Jiang, M. Kammler, F. Ding, Y. Dorenkamp, F. R. Manby, A. M. Wodtke, T. F. Miller, A. Kandratsenka, and O. Bünermann, Science **364**, 379 (2019).
[15] H. Jiang, Y. Dorenkamp, K. Krüger, and O. Bünermann, J. Chem. Phys. **150**, 184704 (2019).
[16] X. Tan, H. Shao, T. Hu, G. Liu, J. Jiang, and H. Jiang, Phys. Chem. Chem. Phys. **17**, 22872 (2015).
[17] D. W. Brenner, O. A. Shenderova, J. A. Harrison, S. J. Stuart, B. Ni, and S. B. Sinnott, J. Phys. Condens. Matter **14**, 783 (2002).
[18] M. E. Fornace, J. Lee, K. Miyamoto, F. R. Manby, and T. F. Miller III, J. Chem. Theory Comput. **11**, 568 (2015).
[19] K. Miyamoto, T. F. Miller III, and F. R. Manby, J. Chem. Theory Comput. **12**, 5811 (2016).
[20] F. Ding, F. R. Manby, and T. F. Miller III, J. Chem. Theory Comput. **13**, 1605 (2017).
[21] X. Tao, P. Shushkov, and T. F. Miller III, J. Chem. Phys. **152**, 124117 (2020).